Mathematical modelling of essential oil supercritical carbon dioxide extraction from chamomile flowers

Oliwer Sliczniuk[a,*], Pekka Oinas[a]

[a]Aalto University, School of Chemical Engineering, Espoo, 02150, Finland

ARTICLE INFO

Keywords:
supercritical extraction
parameter estimation
mathematical modelling

ABSTRACT

This study investigates the supercritical extraction process of essential oil from chamomile flowers. Essential oils of chamomile are used extensively for medicinal purposes. Many different chamomile products have been developed, the most popular of which is herbal tea. In this study, a mathematical model is formulated that describes the governing mass transfer phenomena in a solid–fluid environment under supercritical conditions using carbon dioxide. The concept of quasi-one-dimensional flow is applied to reduce the number of spatial dimensions. The flow of carbon dioxide is assumed to be uniform across any cross-section, although the area available for the fluid phase can vary along the extractor. The physical properties of the solvent are estimated based on the Peng–Robinson equation of state. Model parameters, including the partition factor, internal diffusion coefficient, and decaying factor, were determined through maximum likelihood estimation based on experimental data assuming normally distributed errors. The model parameters were combined to obtain a set of correlations. The generalized process model is capable of reproducing the dataset with satisfactory accuracy.

1. Introduction

Supercritical CO_2 is defined as carbon dioxide that is pressurized and heated above its critical point (31.1 $°C$, 74 bar). Depending on the operating conditions, the fluid properties such as viscosity and density can vary, which leads to multiple industrial applications of CO_2.

The supercritical carbon dioxide is commonly used for impregnation as described by Weidner[1], Machado et al.[2], or Fathi et al.[3] Impregnation is defined as modifying the properties of bulk substances by physically or chemically binding/adsorbing impregnates to a bulk material or surface, such as the hydrophobization of surfaces. The main advantage of using supercritical CO_2 is that it desorbs from the surface and evaporates after depressurization, leaving a solvent-free product. On the other hand, the main disadvantage of using carbon dioxide for impregnation is the low solubility of many drugs of interest.

Another application of supercritical CO_2 is nanoparticles formation as investigated by Padrela et al.[4], Franco and De Marco[5], Saadati Ardestani et al.[6], or Sodeifian et al.[7] Supercritical carbon-dioxide-assisted technologies enable the production of different morphologies of different sizes, including nanoparticles and nanocrystals, by modulating operating conditions. Supercritical fluid-based processes have advantages over techniques conventionally employed to produce nanosized particles or crystals, such as reduced use of toxic solvents. Moreover, the CO_2 is completely removed from the final product by simple depressurization.

One of the most popular applications of supercritical CO_2 is the extraction of essential oils, as described by many researchers, for example, by Sodeifian and Sajadian[8], Reverchon et al.[9], and Sovova[10]. Traditional methods, such as distillation and organic solvent extraction, are commonly employed but have drawbacks. Distillation involves high temperatures that can lead to the thermal degradation of heat-sensitive compounds. This limitation has increased the popularity of alternative techniques, such as supercritical fluid extraction. Supercritical CO_2 is appealing due to its distinctive properties: it is inflammable, non-toxic, and non-corrosive. Supercritical fluids can exhibit both gas- and liquid-like properties, allowing for adjustable dissolving power through changes in operating conditions.

This study investigates the extraction of essential oil from chamomile flowers (Matricaria chamomilla L.) via supercritical fluid extraction techniques and the modelling of this process. Chamomile is a medicinal herb widely cultivated in southern and eastern Europe—in countries such as Germany, Hungary, France, and Russia. It can be found outside Europe, for instance in Brazil, as discussed by Singh et al.[11] This plant is distinguished by its hollow, bright gold cones, housing disc or tubular florets, and being surrounded by about fifteen white ray or ligulate florets. Chamomile has been used for its medicinal benefits, serving as an anti-inflammatory, antioxidant, mild astringent, and healing remedy. Extracts of chamomile are widely used to calm nerves and mitigate anxiety, hysteria, nightmares, insomnia, and other sleep-related conditions, according to Srivastava[12] Orav et al.[13] reported that oil yields from dried chamomile samples ranged from 0.7 to 6.7 mL/kg. The highest yields of essential oil, between 6.1 and 6.7 mL/kg, were derived from chamomile sourced from Latvia and Ukraine. In comparison, chamomile from Armenia exhibited a lower oil content of 0.7 mL/kg.

The literature offers various mathematical models to describe the extraction of valuable compounds from biomass. Selecting a process model is case-to-case dependent and requires analysis of each model's specific assumptions about mass transfer and thermodynamic equilibrium.

*Corresponding author
oliwer.sliczniuk@aalto.fi (O. Sliczniuk)
ORCID(s): 0000-0003-2593-5956 (O. Sliczniuk); 0000-0002-0183-5558 (P. Oinas)

Goto et al.[23] presented the shrinking core (SC) model, which describes a process of irreversible desorption that is followed by diffusion through the pores of a porous solid. When the mass transfer rate of the solute in the non-extracted inner region is significantly slower than in the outer region, where most of the solute has already been extracted, or when the solute concentration exceeds its solubility in the solvent, a distinct boundary may form between the inner and outer regions. As extraction progresses, the core of the inner region shrinks. The model envisions supercritical CO_2 extraction as a sharp, inward-moving front, with a completely non-extracted core ahead of the front and a fully extracted shell behind it.

Sovova[10] proposed the broken-and-intact cell (BIC) model, which assumes that a portion of the solute, initially stored within plant structures and protected by cell walls, is released during the mechanical breakdown of the material. The solute located in the region of broken cells near the particle surface is directly exposed to the solvent, while the core of the particle contains intact cells with undamaged walls. This model describes three extraction phases: a fast extraction phase for accessible oil, a transient phase, and a slow phase controlled by diffusion. The model has been successfully applied to the extraction of grape oil (Sovová et al.[14]) and caraway oil (Sovova et al.[15]).

The supercritical fluid extraction (SFE) process can be be treated similarly to heat transfer, considering solid particles like hot balls cooling down in a uniform environment. Bartle et al.[16] introduced the hot ball diffusion (HBD) model, where spherical particles with uniformly distributed solute diffuse similarly to heat diffusion. Unlike the BIC model, where solute is readily available on the particle surface, the HBD model is suited for systems with small quantities of extractable materials and is not limited by solubility. The model is particularly relevant when internal diffusion controls mass transfer, allowing results from single particles to be extended to the entire bed under uniform conditions. Reverchon et al.[9] have further elaborated on the HBD model and used it to simulate extraction processes for natural materials.

Reverchon[17] proposed a model for extraction of essential oils, which are mainly located inside the vegetable cells in organules called vacuoles. Only a small fraction of essential oil might be near the particle surface due to the breaking up of cells during grinding or in epidermal hairs located on the leaf surface. The fraction of oil freely available on the particle surface should not be significant in the case of SFE from leaves. Consequently, the internal mass-transfer resistance should mainly control the dynamic extraction of essential oil from leaves. Therefore, the external mass-transfer coefficient was neglected in the development of the model of Reverchon[17] The mass balances were developed in the additional hypotheses that the axial dispersion can be neglected and that the solvent density and flow rate are constant along the bed.

This work builds upon the linear kinetic model suggested by Reverchon[17], deriving fundamental governing equations to develop a comprehensive model for the chamomile oil extraction process. This model aims for control-oriented simplicity, assuming a semi-continuous operation within a cylindrical vessel. The process involves a supercritical solvent being pumped through a fixed bed of finely chopped biomass to extract the solute, followed by separation of the solvent and solute in a flush drum to collect the extract. Parameters such as pressure (P), feed flow rate (F), and inlet temperature (T^{in}) are adjustable and measurable, while the outlet temperature (T^{out}) and the amount of product at the outlet can only be monitored. Figure 1 presents a simplified process flow diagram.

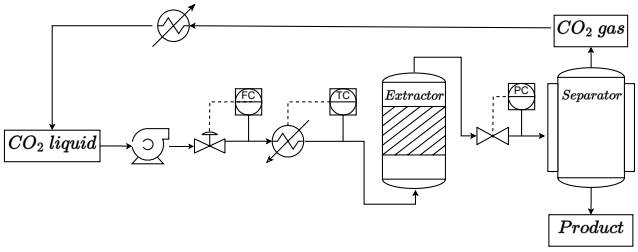

Figure 1: Process flow diagram.

This study aims to develop a process model for extracting natural substances from solid materials using supercritical fluids, with a focus on supercritical CO_2. The approach involves estimating solvent properties through thermodynamic relationships and determining extraction kinetic parameters via a series of experiments conducted under various conditions. This work presents how a classical first-principle model can be modified to a semi-empirical model with mass transfer. Maximum likelihood estimation is used to solve the parameter estimation problem, after which correlations between parameters and operating conditions are established. By identifying these correlations, the process model can be generalized across a broad range of operating conditions. This generalization is a key feature of the presented model and a necessary step for future work, which will utilize the dynamics of the supercritical extraction process.

2. Materials and methods

The extraction of essential oil from chamomile flowers is described by a first principle model given in Section 2.2. The mathematical formulation of the parameter estimation is given in Section 2.3. The process model is tested against the experimental dataset $Y(t)$, which was obtained by extracting oil from chamomile flowers. The experiments were conducted by Povh et al.[26] and Rahimi et al.[27], in a semi-batch extractor with a diameter of 3.96 cm and a length of 16.55 cm. Twelve experiments were performed under different operating conditions: $30 - 40°C$, 100–200 bar, and 0.12–0.24 kg/h. The amount of solid material used for extraction was 75 g.

2.1. Governing equations

Following the work of Anderson[18], the governing equations for a quasi-one-dimensional flow were derived. A quasi-one-dimensional flow refers to a fluid flow scenario assuming that the flow properties are uniformly distributed across any cross-section. This simplification is typically applied when the flow channel's cross-sectional area changes, such as through irregular shapes or partial filling of an extractor. According to this assumption, velocity and other flow properties change solely in the flow direction.

As discussed by Anderson and Cadou[19], all flows are compressible, but some of them can be treated as incompressible when the Mach number is smaller than 0.3. This assumption leads to the incompressible condition: $\nabla \cdot u = 0$, which is valid for constant density (strict incompressible) or varying density flow. The assumption allows for removing acoustic waves and large perturbations in density and/or temperature. In the 1-D case, the incompressibility condition becomes $\frac{du}{dz} = 0$, so the fluid velocity is constant.

The set of quasi-one-dimensional governing equations in Cartesian coordinates is described by Equations 1–3:

$$\frac{\partial\left(\rho_f A_f\right)}{\partial t} + \frac{\partial\left(\rho_f A_f v\right)}{\partial z} = 0 \tag{1}$$

$$\frac{\partial\left(\rho_f v A_f\right)}{\partial t} + \frac{\partial\left(\rho_f A_f v^2\right)}{\partial z} = -A_f \frac{\partial P}{\partial z} \tag{2}$$

$$\frac{\partial\left(\rho_f e A_f\right)}{\partial t} + \frac{\partial\left(\rho_f A_f v e\right)}{\partial z} = -P\frac{\left(A_f v\right)}{\partial z} + \frac{\partial}{\partial z}\left(k\frac{\partial T}{\partial z}\right) \tag{3}$$

where ρ_f is the density of the fluid, A_f is the function which describes a change in the cross-section, v is the velocity, P is the total pressure, e is the internal energy of the fluid, t is time, and z is the spatial direction.

2.2. Extraction model

2.2.1. Continuity equation

The previously derived quasi-one-dimensional continuity equation (Equation 1) is redefined by incorporating the function $A_f = A\phi$. This modification distinguishes constant and varying terms, where the varying term accounts for changes in the cross-sectional area available for the fluid. Equation 4 shows the modified continuity equation:

$$\frac{\partial(\rho_f \phi)}{\partial t} + \frac{\partial(\rho_f v A \phi)}{\partial z} = 0 \tag{4}$$

where A is the total cross-section of the extractor and ϕ describes porosity along the extractor.

Assuming that the mass flow rate is constant in time, the temporal derivative becomes the mass flux F, and the spatial derivative can be integrated along z as follows:

$$\int \frac{\partial(\rho_f v A \phi)}{\partial z} dz = F \rightarrow F = \rho_f v A \phi \tag{5}$$

To simplify the system dynamics, it is assumed that F is a control variable and affects the whole system instantaneously (due to $\nabla \cdot u = 0$), which allows finding the velocity profile that satisfies mass continuity based on F, ϕ, and ρ_f:

$$v = \frac{F}{\rho_f A \phi} \tag{6}$$

Similarly, superficial velocity may be introduced:

$$u = v\phi = \frac{F}{\rho_f A} \tag{7}$$

The fluid density ρ_f can be obtained from an equation of state (Appendix A.1) if the temperature and thermodynamic pressure are known along z. Variation in fluid density may occur due to pressure or inlet temperature changes. In a non-isothermal case, in Equations 6 and 7, ρ_f is considered the average fluid density along the extraction column.

2.2.2. Mass balance for the fluid phase

Equation 8 describes the movement of the solute in the system, which is constrained to the axial direction due to the quasi-one-dimensional assumption. Given that the solute concentration in the solvent is negligible, the fluid phase is described as pseudo-homogeneous, with properties identical to those of the solvent itself. It is also assumed that the thermodynamic pressure remains constant throughout the device. The analysis further simplifies the flow dynamics by disregarding the boundary layer near the extractor's inner wall. This leads to a uniform velocity profile across any cross-section perpendicular to the axial direction. Thus, the mass balance equation includes convection, diffusion, and kinetic terms representing the fluid phase behaviour:

$$\frac{\partial c_f}{\partial t} + \frac{1}{\phi}\frac{\partial\left(c_f u\right)}{\partial z} = \frac{1-\phi}{\phi} r_e + \frac{1}{\phi}\frac{\partial}{\partial z}\left(D_e^M \frac{\partial c_f}{\partial z}\right) \tag{8}$$

where c_f represents the solute concentration in the fluid phase, r_e is the mass transfer kinetic term, and D_e^M is the axial diffusion coefficient.

2.2.3. Mass balance for the solid phase

As given by Equation 9, the solid phase is considered stationary, without convection and diffusion terms in the mass balance equation. Therefore, the only significant term in this equation is the kinetic term of Equation 10, which connects the solid and fluid phases. For simplicity, the extract is represented by a single pseudo-component:

$$\frac{\partial c_s}{\partial t} = \underbrace{r_e}_{\text{Kinetics}} \tag{9}$$

2.2.4. Kinetic term

As the solvent flows through the bed, CO_2 molecules diffuse into the pores and adsorb on the particle surface to form an external fluid film around the solid particles due to the solvent–solid matrix interactions. The dissolved solute diffuses from the particle's core through the solid–fluid interface, the pore, and the film into the bulk. Figure 2 shows the mass transfer mechanism, where the mean solute concentration in the solid phase is denoted as c_s, and the equilibrium concentrations at the solid–fluid interface are denoted as c_s^* and c_p^* for the solid and fluid phases, respectively. The concentration of the solutes in the fluid phase in the centre of the pore is denoted as c_p. As the solute diffuses through the pore, its concentration changes and reaches c_{pf} at the pore opening. Then, the solute diffuses through the film

around the particle and reaches bulk concentration c_f. The two-film theory describes the solid–fluid interface inside the pore. The overall mass transfer coefficient can be determined from the relationship between the solute concentration in one phase and its equilibrium concentration.

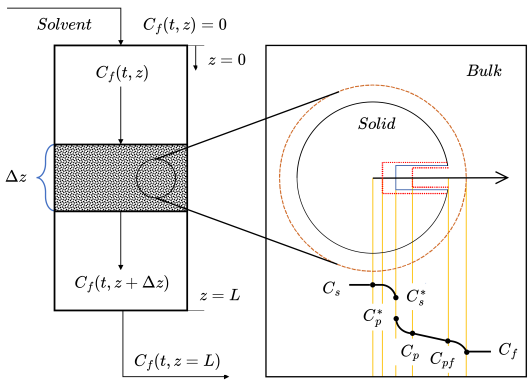

Figure 2: Mass transfer mechanism.

Bulley et al.[20] suggest a process where the driving force for extraction is given by the difference between the concentration of the solute in the bulk, c_f, and in the centre of the pore, c_p^*. The concentration c_p^* is in equilibrium with c_s according to the equilibrium relationship. The rate of extraction is thus $r_e\left(c_f - c_p^*(c_s)\right)$. In contrast, Reverchon[17] proposes a driving force given by the difference between c_s and c_p^*. Concentration c_p^* is determined by the equilibrium relationship with c_f and the extraction rate given by Equation 10:

$$r_e = \frac{D_i}{\mu l^2}\left(c_s - c_p^*\right) \tag{10}$$

where μ is sphericity, l a characteristic dimension of particles that can be defined as $l = r/3$, r is the mean particle radius, ρ_s is the solid density, D_i corresponds to the overall diffusion coefficient, and c_P^* is the concentration at the solid–fluid interface (which according to the internal resistance model is supposed to be at equilibrium with the fluid phase).

According to Bulley et al.[20], a linear equilibrium relationship (Equation 11) can be used to find the equilibrium concentration of the solute in the fluid phase c_f^* based on the concentration of the solute in the solid phase c_s:

$$c_f^* = k_p c_s \tag{11}$$

The volumetric partition coefficient k_p acts as an equilibrium constant between the solute concentration in one phase and the corresponding equilibrium concentration at the solid–fluid interphase. According to Spiro[21], k_p can be expressed through the mass partition coefficient k_m:

$$k_m = \frac{k_p \rho_s}{\rho_f} \tag{12}$$

According to Reverchon[17], the kinetic term becomes:

$$r_e = -\frac{D_i}{\mu l^2}\left(c_s - \frac{\rho_s c_f}{k_m \rho_f}\right) \tag{13}$$

2.2.5. *Distribution of uneven solute in the solid phase*

Following the idea of the BIC model (Sovova[22]), the internal diffusion coefficient D_i is considered to be a product of the reference value of D_i^R and the exponential decay function γ, as given by Equation 14:

$$D_i = D_i^R \gamma(c_s) = D_i^R \exp\left(\Upsilon\left(1 - \frac{c_s}{c_{s0}}\right)\right) \tag{14}$$

where Υ describes the curvature of the decay function. Equation 15 describes the final form of the kinetic term:

$$r_e = -\frac{D_i^R \gamma}{\mu l^2}\left(c_s - \frac{\rho_s c_f}{k_m \rho_f}\right) \tag{15}$$

The γ function limits the solute's availability in the solid phase. Similarly to the BIC model, the solute is assumed to be contained in the cells, some of which are open because the cell walls were broken by grinding, with the rest remaining intact. The diffusion of the solute from a particle's core takes more time than the diffusion of the solute close to the outer surface. The same idea can be represented by the decaying internal diffusion coefficient, where the decreasing term is a function of the solute concentration in the solid.

Alternatively, the decay function γ can be interpreted by referring to the SC model presented by Goto et al.[23], where the particle radius changes as the amount of solute in the solid phase decreases. As the particle size decreases due to dissolution, the diffusion path increases, which makes the diffusion slower and reduces the value of the diffusion coefficient. This analogy can be applied to Equation 14 to justify the application of a varying diffusion coefficient.

2.2.6. *Extraction yield*

The process yield is calculated according to Equation 16 as presented by Sovova et al.[15]. The measurement equation evaluates the solute's mass at the extraction unit outlet and sums it up. The integral form of the measurement (Equation 16) can be transformed into the differential form (Equation 17) and augmented with the process model.

$$y = \int_{t_0}^{t_f} \frac{F}{\rho_f} c_f \Big|_{z=L} dt \tag{16}$$

$$\frac{dy}{dt} = \frac{F}{\rho_f} c_f \Big|_{z=L} \tag{17}$$

2.2.7. *Initial and boundary conditions*

It is assumed that the solvent is free of solute at the beginning of the process $c_{f0} = 0$, that all the solid particles have the same initial solute content c_{s0}, and that the system is isothermal. The fluid at the inlet is also considered not to contain any solute. As the residence time is much shorter than the sampling time, the initial state estimate for the solute concentration in the fluid phase would be unreliable. The initial and boundary conditions are defined as follows:

$$c_f(t=0,z)=0 \qquad c_s(t=0,z)=c_{s0} \qquad c_f(t,z=0)=0$$
$$\frac{\partial c_f(t,z=L)}{\partial x}=0 \qquad c_s(t,z=\{0,L\})=0 \qquad y(0)=0$$

2.2.8. *Discretization methods*

The method of lines is used to transform the process model equations into a set of ODEs denoted as $G(x;\Theta)$. The backward finite difference is used to approximate the first-order derivative, while the central difference scheme approximates the second-order derivative z direction. The length of the fixed bed is divided into N_z, that is, equally distributed points in the z direction. The state-space model after discretization is denoted as x and defined as follows:

$$\dot{x} = \frac{dx}{dt} = \begin{bmatrix} \frac{dc_{f,1}}{dt} \\ \vdots \\ \frac{dc_{f,N_z}}{dt} \\ \hline \frac{dc_{s,1}}{dt} \\ \vdots \\ \frac{dc_{s,N_z}}{dt} \\ \hline \frac{dy(t)}{dt} \end{bmatrix} = \underbrace{\begin{bmatrix} G_1\left(c_f, c_s; \Theta\right) \\ \vdots \\ G_{N_z}\left(c_f, c_s; \Theta\right) \\ \hline G_{N_z+1}\left(c_f, c_s; \Theta\right) \\ \vdots \\ G_{2N_z}\left(c_f, c_s; \Theta\right) \\ \hline G_{2N_z+2}\left(c_f, c_s; \Theta\right) \end{bmatrix}}_{G(x;\Theta)}$$

where $x \in \mathbb{R}^{N_x=2N_z+1}$ and $\Theta \in \mathbb{R}^{N_\Theta=N_\theta+N_u}$, N_θ is the number of parameters and N_u is the number of control variables.

For a derivative to be conservative, it must form a telescoping series. In other words, only the boundary terms should remain after adding all terms coming from the discretization over a grid, and the artificial interior points should be cancelled out. Discretization is applied to the conservative form of the model to ensure mass conservation.

2.3. Parameter estimation

Only some of the parameters in a process model can be estimated from the theoretical considerations. Parameter estimation aims to obtain the "best" estimate of unknown parameters θ (a subset of the parameter space Θ containing all model parameters) based on continuous observations or the discrete. The unobservable error $\epsilon(t)$ is added to the deterministic model output, $y(t)$, to give the observable dependent variable $Y(t)$. For discrete observations, this can be expressed as follows:

$$Y(t_i) = y(\theta, t_i) + \epsilon(t_i)$$

For continuous variables, the equation is as follows:

$$Y(t) = y(\theta, t) + \epsilon(t)$$

However, obtaining analytical solutions for a deterministic process model can be challenging, so experiments are often conducted where the vector of derivatives $\frac{dY(t_i)}{dt}$ is measured instead of $Y(t_i)$ itself. In such cases, it is assumed that the unobservable error is added to the deterministic derivative $\frac{dy(\theta,t_i)}{dt}$ as shown below:

$$\frac{dY(t_i)}{dt} = \frac{dy(\theta, t_i)}{dt} + \epsilon(t_i) \tag{18}$$

In a case where the error in the first observation is denoted as ϵ_1, the error in the second observation ϵ_2' incorporates ϵ_1 as well as an independent random component, given by $\epsilon_2' = \epsilon_1 + \epsilon_2$. Similarly, the error in the third observation is $\epsilon_3' = \epsilon_1 + \epsilon_2 + \epsilon_3$, and so forth. Mandel[24] made a distinction between the typically assumed independent measurement error in the dependent variable and a "cumulative" or interval error, in which each new observation encompasses the error of the previous ones. Cumulative errors arise from fluctuations in the process due to small variations in operating conditions and are not independent; only the differences in measurement from one period to the next are independent.

Maximum likelihood estimation (MLE) is a statistical method used to estimate the parameters of a probability distribution based on observed data. MLE works by finding the values of the parameters that maximize the likelihood function, which is the probability of observing the given data for a given set of parameter values. MLE has desirable properties such as asymptotic efficiency and normality. Although MLE has often been associated with the normal distribution for mathematical convenience, it can be applied to a wide range of probability distributions. The derivation of the likelihood function under the assumption of Gaussian distribution is discussed by Himmelblau[25]. The objective function is presented by Equation 19:

$$\ln \mathcal{L} = -\frac{n}{2}\ln\left(2\pi\sigma^2\right) - \frac{\sum_{i=1}^{n}\left[\frac{dY(t_i)}{dt} - \frac{dy(\theta,t_i)}{dt}\right]^2}{2\sigma^2} \tag{19}$$

The parameter estimation problem can be formulated as follows:

$$\begin{aligned} \hat{\theta}_{MLE} &= \arg\max_{\sigma,\theta\in\Theta} \ln \mathcal{L} = \arg\max_{\sigma,\theta\in\Theta} p(\theta|y) \\ \text{subject to} \quad \dot{x} &= G(x;\Theta(\theta)) \\ \dot{\theta} &= 0 \\ y &= y(t) \\ \theta^{lb} &\le \theta \le \theta^{ub} \end{aligned} \tag{20}$$

where $\hat{\theta}$ is the maximum likelihood estimator, θ^{lb} defines the minimal value of θ, θ^{ub} is the maximum value of θ, and σ represents the standard deviation of the residuals (errors) between the dataset and the model outputs.

The initial guess for each decision variable, as well as the lower and upper bounds, are given in Table 1.

Parameter	k_m[-]	$D_i^R \cdot 10^{-13}[m^2/s]$	Υ [-]	σ
Lower bound	0	0	0	0
Upper bound	$+\infty$	$+\infty$	$+\infty$	$+\infty$
Initial guesses	0.1-10	$0.1-10$	0.1-10	0.1-10

Table 1: Constraints and initial guess.

The solution of Equation 20 yields the estimates $\hat{\theta}$. For some models, these equations can be explicitly solved for $\hat{\theta}$, but in general, no closed-form solution to the maximization problem is known or available, and a maximum likelihood estimator can only be found via numerical optimization.

3. Results

To solve the parameter estimation problem, the single shooting method was used to transform the boundary-value problem into the initial value problem and to formulate the non-linear programming problem. This non-linear optimisation task was tackled using the CasADi framework (Andersson et al.[28]). Each time series was fitted separately to the model with the linear extraction kinetics (Equation 13). The parameter estimation problem was solved multiple times with varying parameter initial values to identify the global minimum. In the case of linear kinetic, two parameters remain to be determined: the partition coefficient k_m and the internal diffusion coefficient D_i. Rahimi et al.[27] analyzed the same dataset and reported Peclet numbers between 290 and 400. A high Peclet number suggests that the advection term dominates the mass transfer, and the axial diffusion is negligible, which is one of the modelling assumptions.

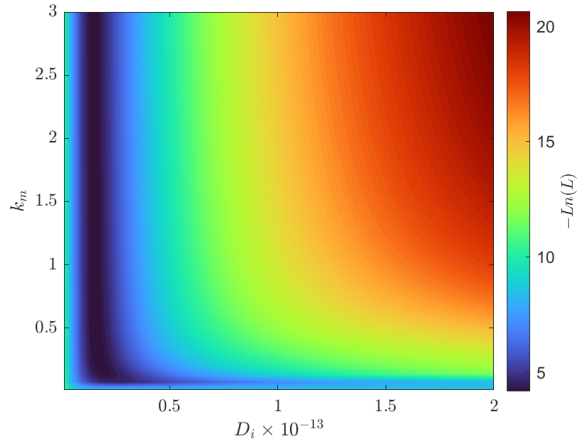

(a) The linear kinetic model.

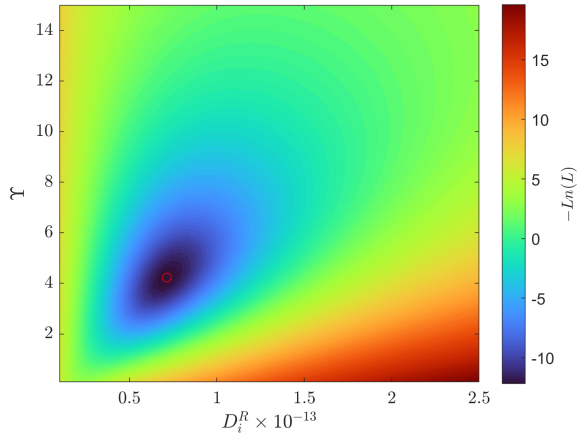

(b) The modified model.

Figure 3: Parameter space for experiment 1.

Figure 3a shows the parameter space and corresponding values of the cost function for experiment 1 ($40°C$, 100 bar and $6.67{\cdot}10^{-5}$ kg/s). A black-coloured section, in the shape of a vertical stripe at $D_i \approx 0.2$, indicates the minimum values of the cost function $-\ln(L)$. In the direction of k_m, the cost function is almost flat, which suggests that any value of k_m above 0.1 fits the data equally well. If k_m can be an arbitrary point, then it can grow to infinity, which suggests that the solvent is far from saturation, and the model can be simplified. The model reduction can be introduced by considering the limit of k_m:

$$\lim_{k_m \to \infty} \left(c_s(t,z) - \frac{\rho_s}{k_m(T(t,z))\rho(T(t,z),P(t))} c_f \right) =$$

$$= \left(c_s(t,z) - \frac{\rho_s}{\infty \cdot \rho(T(t,z),P(t))} c_f(t,z) \right) = \left(c_s(t,z) - 0 \right)$$

In the scenario previously discussed, the fitting outcomes were not deemed satisfactory. Building upon the concepts underlying the BIC and SC models (detailed in Section 2.2.5), the γ function is introduced to capture the decreasing extraction kinetics. The correction factor is combined with the simplified linear model, resulting in a two-parameter model (D_i^R and Υ) as given by Equation 15. Figure 3b shows the parameter space and the corresponding cost function values.

The parameter space for the modified model exhibits a distinct minimum value corresponding to the solution of the parameter estimation problem for experiment 1. The red circle highlights the minimum value of the cost function found by the optimizer. The remaining experiments are fitted to the modified extraction model, and the results, presented in Figure 4, show good agreement with the dataset.

The parameter estimation results are combined to analyze the relationship between the obtained parameters and the operating conditions. Unlike traditional methods that employ a combination of Reynolds, Schmidt, and Sherwood numbers to find correlation, the approach in this study leverages the fixed-bed Reynolds number $\left(Re = \frac{2r \cdot \rho_f \cdot u}{\mu} \right)$ as the independent variable. The Reynolds number has the advantage of considering the influence of all the control variables (temperature, pressure, and flow rate), which means it can be uniquely defined by selecting the operating conditions.

In Figures 5a and 5b, two distinct data clusters emerge, each corresponding to a different mass flow rate. Despite the linear trends observed in both sets of correlations, the data points for D_i^R decrease with increasing Re, while those for Υ increase with Re. The reduction of D_i^R with an increase of Re can be attributed to higher fluid density and increased mass transfer resistance.

A more general relationship can be obtained by applying multiple linear regression instead of linear regression. The data clusters in Figure 5a and 5b are close to parallel, suggesting that a plane would combine all the data points. The Reynolds number and mass flow rate act as independent variables for D_i^R and Υ, as presented in Figures 6a and 6b. The presented correlations are valid in the whole range of investigated operating conditions. The correlations are later tested against the original dataset to show that the correlations can reproduce the results with satisfactory accuracy. Figure 7 shows the results of the simulations with incorporated correlations. Good agreement between the simulation results and the dataset can be observed, as presented by low values of the mean square error and standard deviation as

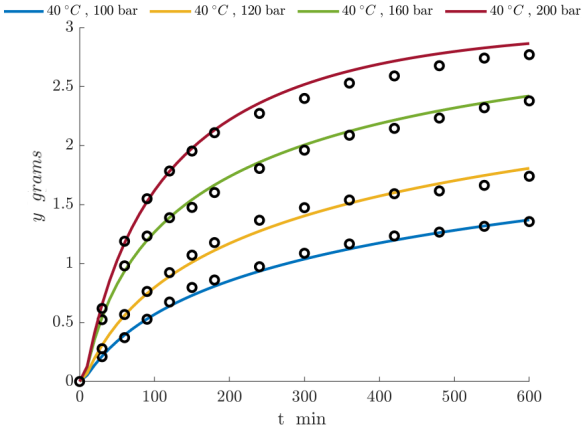

(a) Parameter estimation results at $6.67 \cdot 10^{-5}$ kg/s and temperature of 40 °C.

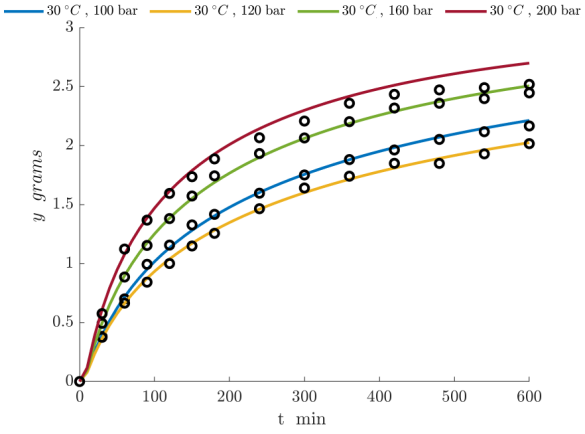

(b) Parameter estimation results at $6.67 \cdot 10^{-5}$ kg/s and temperature of 30 °C.

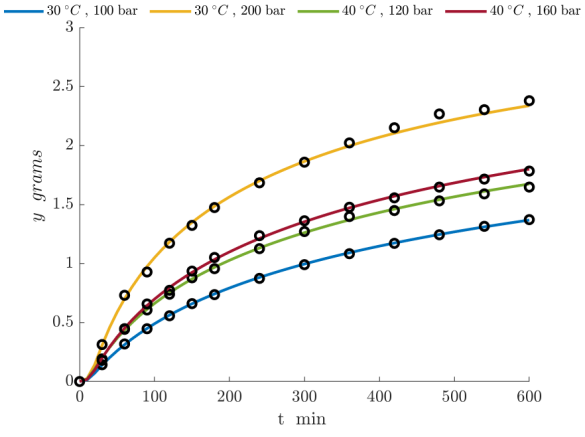

(c) Results of parameter estimation for experiments at $3.33 \cdot 10^{-5}$ kg/s.

Figure 4: Parameter estimation results obtained from the modified model.

presented in Table 2. If Figures 4 and 7 are compared, a decrease in the accuracy of simulations can be observed. Such behaviour is expected due to the bias–variance trade-off, which describes the relationship between a model's complexity and the accuracy of its predictions.

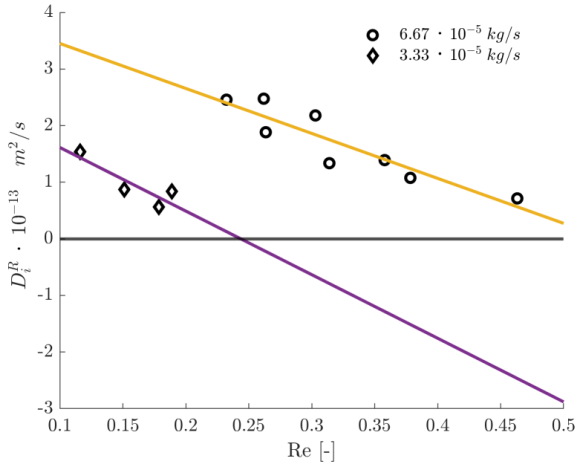

(a) Linear regression $D_i^R = f(Re)$.

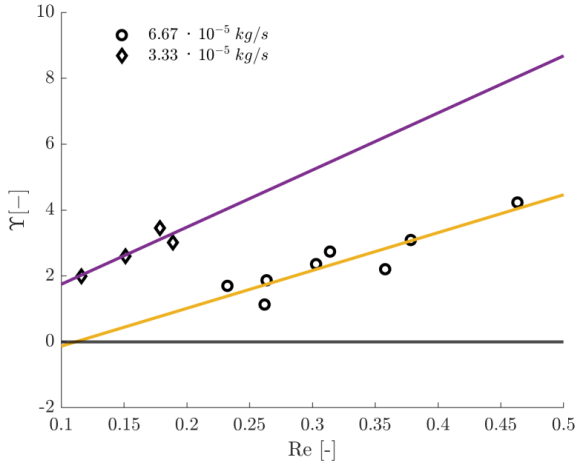

(b) Linear regression $\Upsilon = f(Re)$.

Figure 5: Linear correlations between parameters.

The parameter estimation results are compared against those presented by Povh et al.[26], who applied the Sovova model to the same dataset. It is important to note that, as the initial solute mass ratio, Povh et al.[26] used a value of 10% above the total amount of extract for every experiment, while in this work, the initial conditions are the same for all the experiments. In contrast to this work, Povh et al.[26] did not utilise numerical solvers but used a mix of analytical methodologies and trial-and-error procedures. Povh et al.[26] remarked that 'the direct fitting of experimental data to Sovova's model produced parameters that could not be accepted after a careful physical interpretation of the system'. The parameters identified in this study have a physical interpretation and are within the expected range.

Rahimi et al.[27] analyzed the same dataset using the desorption–dissolution–diffusion model. To decrease the number of unknown parameters, Rahimi et al.[27] applied a set of empirical correlations. The remaining parameters were determined using a genetic algorithm to solve the parameter estimation problem for each experiment individually. The results obtained by Rahimi et al.[27] show that the desorption–dissolution–diffusion model fails to reproduce the yield data.

Experiment	1	2	3	4	5	6	7	8	9	10	11	12
Mean squared error of the cumulative measurement	0.0178	0.0058	0.0027	0.0361	0.0162	0.0596	0.0162	0.0296	0.0420	0.0295	0.0083	0.0048
Mean squared error of the independent measurements	0.0007	0.0010	0.0013	0.0023	0.0008	0.0021	0.0010	0.0016	0.0007	0.0014	0.0005	0.0005
Standard deviation of error of the independent measurements	0.0255	0.0309	0.0369	0.0488	0.0269	0.0418	0.0296	0.0356	0.0169	0.0345	0.0214	0.0212

Table 2: Error between experimental data and model predictions.

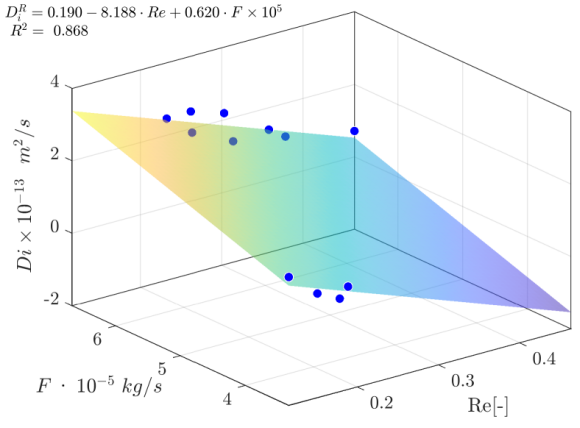

(a) Multiple linear regression $D_i^R = f(Re, F)$.

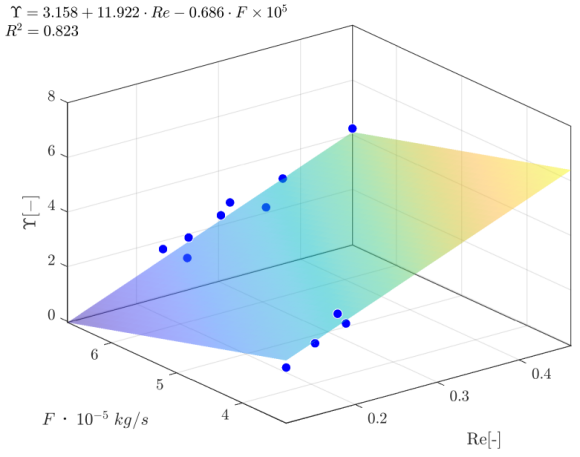

(b) Multiple linear regression $\Upsilon = f(Re, F)$.

Figure 6: Empirical correlations between parameters.

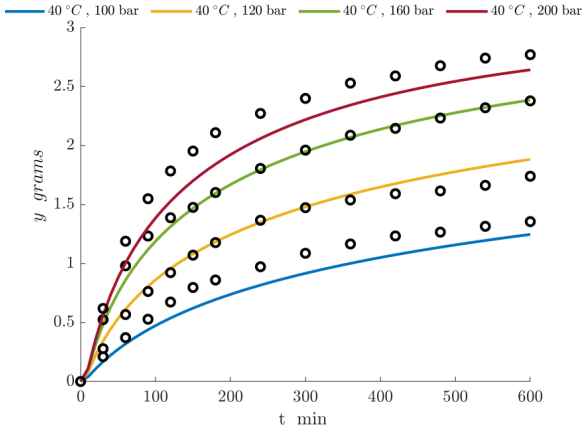

(a) Simulation results obtained at $6.67 \cdot 10^{-5}$ kg/s and temperature of 40 °C.

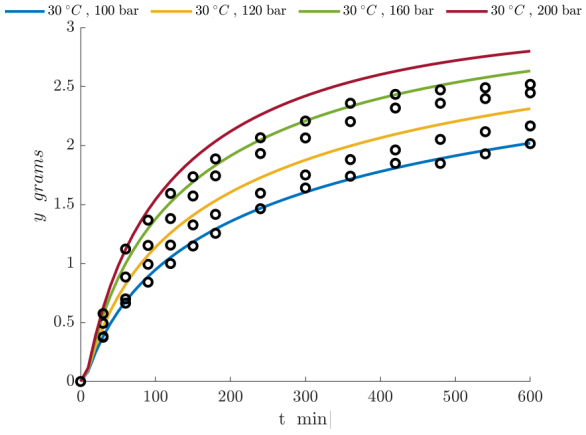

(b) Simulation results obtained at $6.67 \cdot 10^{-5}$ kg/s and temperature of 30 °C.

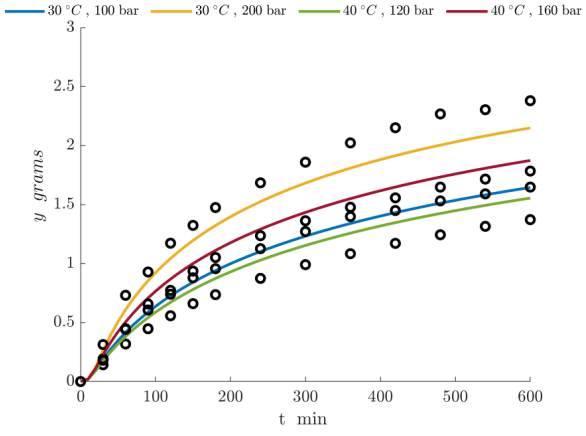

(c) Simulation results obtained at $3.33 \cdot 10^{-5}$ kg/s

Figure 7: Simulation results from the modified model and correlations.

The main difference between the model employed by Rahimi et al.[27] and the one in this study is the γ function. The γ function increases the model's flexibility by adjusting D_i and allows it to obtain a better fit. Povh et al.[26] and Rahimi et al.[27] delivered a set of independent parameters for every experiment. This work combines the parameters obtained from each experiment to obtain a single correlation valid for the whole range of investigated operating conditions.

The primary advantage of the proposed model lies in its added flexibility compared to traditional desorption–dissolution–diffusion models found in the literature. While it follows the same assumptions and limitations as these traditional models, it introduces an additional postulate: a decaying internal diffusion coefficient. If there is no actual decay in D_i, the presented model can approximate the traditional desorption–dissolution–diffusion models by finding low values of a decaying factor Υ. In such a case, the

exponent approach unity as Υ goes to zero regardless of $\left(1 - \frac{c_s}{c_{s0}}\right)$. This added flexibility, however, comes at the cost of requiring an extra parameter to be fitted, which could lead to overfitting, especially with limited datasets.

The model modification was not derived from theoretical considerations but from analyzing assumptions in existing models, such as the BIC model and the SC model, and applying corresponding simplifications. As a result, the proposed model should be categorized as semi-empirical. This approach allows for the development of tailored models but may make finding physical interpretations for some parameters challenging.

The accuracy of the obtained correlations is heavily influenced by the quality of the dataset and the number of experiments conducted under different operating conditions. A significant limitation is that the dataset was obtained from static experiments (constant operating conditions). Performing a set of experiments under dynamically changing operating conditions would provide more information about the unknown parameters and system dynamics.

4. Conclusions

The article has presented a comprehensive study on the supercritical fluid extraction of essential oil from chamomile flowers, focusing on developing and applying a distributed-parameter model to describe the fluid–solid extraction process. By employing the concept of quasi-one-dimensional flow, the study simplifies the spatial dimensions of the extraction process, ensuring uniform flow across any cross-section while allowing for variations in the area available for the fluid phase. The physical properties of the solvent are estimated using the Peng–Robinson equation of state.

The model calibration is based on the data from laboratory experiments conducted by Povh et al.[26] under various conditions. The model parameters, such as the partition factor, internal diffusion coefficient, and decaying factor, were determined through maximum likelihood estimation based on experimental data. The parameter space exploration revealed that while some parameters could be determined with a high degree of confidence, others, like the partition factor, had a low impact on the model's output. The identification of low-impact parameters leads to model reduction. This work introduced a set of correlations to find a relationship between the kinetic parameters and the operating conditions. The obtained correlations were incorporated into the process model and tested against the dataset. The process model is capable of reproducing the dataset with satisfactory accuracy.

References

[1] Eckhard Weidner. Impregnation via supercritical co2–what we know and what we need to know. The Journal of Supercritical Fluids, 134: 220–227, April 2018. ISSN 0896-8446. doi: 10.1016/j.supflu.2017.12.024.

[2] Noelia D. Machado, José E. Mosquera, Raquel E. Martini, María L. Goñi, and Nicolás A. Gañán. Supercritical co2-assisted impregnation/deposition of polymeric materials with pharmaceutical, nutraceutical, and biomedical applications: A review (2015–2021). The Journal of Supercritical Fluids, 191:105763, December 2022. ISSN 0896-8446. doi: 10.1016/j.supflu.2022.105763.

[3] Mostafa Fathi, Gholamhossein Sodeifian, and Seyed Ali Sajadian. Experimental study of ketoconazole impregnation into polyvinyl pyrrolidone and hydroxyl propyl methyl cellulose using supercritical carbon dioxide: Process optimization. The Journal of Supercritical Fluids, 188:105674, September 2022. ISSN 0896-8446. doi: 10.1016/j.supflu.2022.105674.

[4] Luís Padrela, Miguel A. Rodrigues, Andreia Duarte, Ana M.A. Dias, Mara E.M. Braga, and Hermínio C. de Sousa. Supercritical carbon dioxide-based technologies for the production of drug nanoparticles/nanocrystals – a comprehensive review. Advanced Drug Delivery Reviews, 131:22–78, June 2018. ISSN 0169-409X. doi: 10.1016/j.addr.2018.07.010.

[5] Paola Franco and Iolanda De Marco. Nanoparticles and nanocrystals by supercritical co2-assisted techniques for pharmaceutical applications: A review. Applied Sciences, 11(4):1476, February 2021. ISSN 2076-3417. doi: 10.3390/app11041476.

[6] Nedasadat Saadati Ardestani, Gholamhossein Sodeifian, and Seyed Ali Sajadian. Preparation of phthalocyanine green nano pigment using supercritical co2 gas antisolvent (gas): experimental and modeling. Heliyon, 6(9):e04947, September 2020. ISSN 2405-8440. doi: 10.1016/j.heliyon.2020.e04947.

[7] Gholamhossein Sodeifian, Seyed Ali Sajadian, and Reza Derakhsheshpour. Co2 utilization as a supercritical solvent and supercritical antisolvent in production of sertraline hydrochloride nanoparticles. Journal of CO2 Utilization, 55:101799, January 2022. ISSN 2212-9820. doi: 10.1016/j.jcou.2021.101799.

[8] Gholamhossein Sodeifian and Seyed Ali Sajadian. Investigation of essential oil extraction and antioxidant activity of echinophora platyloba dc. using supercritical carbon dioxide. The Journal of Supercritical Fluids, 121:52–62, March 2017. ISSN 0896-8446. doi: 10.1016/j.supflu.2016.11.014.

[9] E. Reverchon, G. Donsi, and L.S. Osseo. Modeling of supercritical fluid extraction from herbaceous matrices. Industrial & Engineering Chemistry Research, 32(11):2721–2726, 1993. doi: 10.1021/ie00023a039.

[10] H. Sovova. Rate of the vegetable oil extraction with supercritical co_2. modelling of extraction curves. Chemical Engineering Science, 49 (3):409–414, 1994. doi: 10.1016/0009-2509(94)87012-8.

[11] O. Singh, Z. Khanam, N. Misra, and M. Srivastava. Chamomile (matricaria chamomilla l.): An overview. Pharmacognosy Reviews, 5 (9):82, 2011. ISSN 0973-7847. doi: 10.4103/0973-7847.79103.

[12] J. Srivastava. Extraction, characterization, stability and biological activity of flavonoids isolated from chamomile flowers. Molecular and Cellular Pharmacology, 1(3):138–147, 2009. ISSN 1938-1247. doi: 10.4255/mcpharmacol.09.18.

[13] A. Orav, A. Raal, and E. Arak. Content and composition of the essential oil of chamomilla recutita(l.) rauschert from some european countries. Natural Product Research, 24(1):48–55, 2010. ISSN 1478-6427. doi: 10.1080/14786410802560690.

[14] H. Sovová, J. Kučera, and J. Jež. Rate of the vegetable oil extraction with supercritical co2—ii. extraction of grape oil. Chemical Engineering Science, 49(3):415–420, 1994. ISSN 0009-2509. doi: 10.1016/0009-2509(94)87013-6.

[15] H. Sovova, R. Komers, J. Kucuera, and J. Jezu. Supercritical carbon dioxide extraction of caraway essential oil. Chemical Engineering Science, 49(15):2499–2505, 1994. doi: 10.1016/0009-2509(94)e0058-x.

[16] Keith D. Bartle, Anthony A. Clifford, Steven B. Hawthorne, John J. Langenfeld, David J. Miller, and Robert Robinson. A model for dynamic extraction using a supercritical fluid. The Journal of Supercritical Fluids, 3(3):143–149, September 1990. ISSN 0896-8446. doi: 10.1016/0896-8446(90)90039-o.

[17] E. Reverchon. Mathematical modeling of supercritical extraction of sage oil. AIChE Journal, 42(6):1765–1771, 1996. doi: 10.1002/aic.690420627.

[18] J. Anderson. Computational fluid dynamics : the basics with applications. McGraw-Hill, 1995. ISBN 9780071132107.

[19] J. Anderson and Ch. Cadou. Fundamentals of Aerodynamics. McGraw-Hill Education, 2023. ISBN 9781264151929.

[20] N. R. Bulley, M. Fattori, A. Meisen, and L. Moyls. Supercritical fluid extraction of vegetable oil seeds. Journal of the American Oil Chemists' Society, 61(8):1362–1365, 1984. doi: 10.1007/bf02542243.

[21] M. Spiro. Extraction of ginger rhizome: partition constants and other equilibrium properties in organic solvents and in supercritical carbon dioxide. International Journal of Food Science & Technology, 25(5): 566–575, 2007. doi: 10.1111/j.1365-2621.1990.tb01116.x.

[22] H. Sovova. Broken-and-intact cell model for supercritical fluid extraction: Its origin and limits. The Journal of Supercritical Fluids, 129:3–8, 2017. doi: 10.1016/j.supflu.2017.02.014.

[23] M. Goto, B. C. Roy, and T. Hirose. Shrinking-core leaching model for supercritical-fluid extraction. The Journal of Supercritical Fluids, 9(2):128–133, 1996. doi: 10.1016/s0896-8446(96)90009-1.

[24] J. Mandel. Fitting a straight line to certain types of cumulative data. Journal of the American Statistical Association, 52(280):552–566, 1957. doi: 10.1080/01621459.1957.10501413.

[25] D. Himmelblau. Process analysis by statistical methods, 1970. [by] David M. Himmelblau., Includes bibliographical references.

[26] N. P. Povh, M. O. M. Marques, and M. A. A. Meireles. Supercritical co_2 extraction of essential oil and oleoresin from chamomile (chamomilla recutita [l.] rauschert). The Journal of Supercritical Fluids, 21(3):245–256, 2001. ISSN 0896-8446. doi: 10.1016/s0896-8446(01)00096-1.

[27] E. Rahimi, J.M. Prado, G. Zahedi, and M.A.A. Meireles. Chamomile extraction with supercritical carbon dioxide: Mathematical modeling and optimization. The Journal of Supercritical Fluids, 56(1):80–88, 2011. ISSN 0896-8446. doi: 10.1016/j.supflu.2010.11.008.

[28] J. A. E. Andersson, J.Gillis, G. Horn, J. B. Rawlings, and M. Diehl. CasADi: a software framework for nonlinear optimization and optimal control. Mathematical Programming Computation, 11(1):1–36, 2018. doi: 10.1007/s12532-018-0139-4.

[29] D-Y. Peng and D. B. Robinson. A new two-constant equation of state. Industrial & Engineering Chemistry Fundamentals, 15(1):59–64, 1976. doi: 10.1021/i160057a011.

[30] J. Gmehling, M. Kleiber, B. Kolbe, and J. Rarey. Chemical Thermodynamics for Process Simulation. Wiley, 2019. doi: 10.1002/9783527809479.

A. Appendix

A.1. Equation of state

A cubic equation of state (EoS) serves as a mathematical model to describe the behaviour of real gases and liquids through a third-degree polynomial equation that correlates a substance's pressure, volume and temperature. These equations constitute tools for comprehending phase behaviour, properties, and thermodynamic processes of real substances across various engineering and scientific applications. The cubic equation of state takes into account deviations from ideal gas behaviour, which are particularly important at high pressures and low temperatures, where real gases do not follow the assumption of an ideal gas.

$$P = \frac{RT}{v_m - b} - \frac{\Phi}{v_m^2 - ubv_m + wb^2} \tag{21}$$

In this equation, P denotes the pressure of the substance, v_m represents the molar volume of the substance, T stands for the absolute temperature of the substance, u and w are integers that vary from one equation to another, R symbolizes the universal gas constant, ω denotes an acentric factor, and $\Phi = a\alpha$.

The Van der Waals constants constitute empirical values contingent upon the particular substance being modelled. These constants factor in molecular interactions (represented by 'a') and the finite size of gas molecules (indicated by 'b').

Several variations of the cubic equation of state exist, each with its own set of parameters and assumptions. Tables 3 and 4 show parameters for popular cubic EoS.

EoS	u	w	a	b
van der Waals	0	0	$\frac{27}{64}\frac{R^2T_c^2}{P_c}$	$\frac{RT_c}{8P_c}$
Redlich and Kwong	1	0	$0.42748\frac{R^2T_c^{2.5}}{P_c}$	$\frac{0.08664RT_c}{P_c}$
Soave	1	0	$0.42748\frac{R^2T_c^2}{P_c}$	$\frac{0.08664RT_c}{P_c}$
Peng and Robinson[29]	2	-1	$0.45724\frac{R^2T_c^2}{P_c}$	$\frac{0.07780T_c}{P_c}$

Table 3: Parameters for popular cubic EoS.

EoS	α	f(ω)
van der Waals	-	-
Redlich and Kwong	$\frac{1}{\sqrt{T_r}}$	-
Soave	$\left[1 + f(\omega)\left(1 - \sqrt{T_r}\right)\right]^2$	0.48+1.574ω-0.176ω^2
Peng and Robinson ([29])	$\left[1 + f(\omega)\left(1 - \sqrt{T_r}\right)\right]^2$	0.37464+1.54226ω-0.26992ω^2

Table 4: Parameters for popular cubic EoS.

The general cubic equation of state can be represented as a polynomial, as indicated in Equation 22. In a one-phase region, the fluid is characterized by a single real root corresponding to the gas, liquid, or supercritical phase. In the two-phase region, a gas–liquid mixture exists, and two roots are identified. The larger root corresponds to the gas phase, while the smaller root pertains to the liquid phase.

$$Z^3 - (1 + B - uB)Z^2 + (A + wB^2 - uB - uB^2)Z - AB - wB^2 - wB^3 = 0 \tag{22}$$

where $A = \frac{\Phi P}{R^2T^2}$ and $B = \frac{bP}{RT}$.

If the Peng–Robinson equation of state (Peng and Robinson[29]) is used, the polynomial equation becomes:

$$Z^3 - (1 - B)Z^2 + (A - 2B - 3B^2)Z - (AB - B^2 - B^3) = 0 \tag{23}$$

For an ideal gas, the compressibility factor is defined as $Z = 1$, but the deviation of Z needs to be considered for real-life cases. The value of Z typically increases with pressure and decreases with temperature. At elevated pressures, molecules collide more frequently, which allows the repulsive forces between molecules to influence the molar volume of the real gas (v_m), making it surpass that of the corresponding ideal gas $\left(\left(v_m\right)_{ideal\ gas} = \frac{RT}{P}\right)$, resulting in Z exceeding one. At lower pressures, molecules move freely, with attractive forces predominating, leading to $Z < 1$.

Numerical methods such as Newton–Raphson can be used to solve the polynomial equation to obtain the compressibility $Z\,(T(t, z), P(t))$ at a given temperature and pressure. Alternatively, a closed-form solution can be obtained by using the Cardano formula (Appendix A.2).

A.1.1. Density of the fluid phase

The density of the fluid can be calculated from the real gas equation $\rho = \frac{P}{RTZ}\frac{1}{m_{CO2}}$. The temperature can be obtained from the time evolution of governing equations, and the pressure is considered to be constant along the system.

A.2. Cardano's formula

Following the work of Gmehling et al.[30], a cubic equation of state can be written in the following form:

$$Z^3 + UZ^2 + SZ + T = 0 \tag{24}$$

where Z is the compressibility factor. Cubic equations can be solved analytically using Cardano's formula:

$$P = \frac{3S - U^2}{3} \qquad Q = \frac{2U^3}{27} - \frac{US}{3} + T$$

The discriminant can be determined to be:

$$D = \left(\frac{P}{3}\right)^3 + \left(\frac{Q}{2}\right)^2 \tag{25}$$

For $D > 0$, the equation of state has one real solution:

$$Z = \left[\sqrt{D} - \frac{Q}{2}\right]^{1/3} - \frac{P}{3\left[\sqrt{D} - \frac{Q}{2}\right]^{1/3}} - \frac{U}{3} \tag{26}$$

For $D < 0$, there are three real solutions:

$$\Theta = \sqrt{-\frac{P^3}{27}} \qquad \Phi = \arccos\left(\frac{-Q}{2\Theta}\right)$$

They can be written as follows:

$$Z_1 = 2\Theta^{(1/3)}\cos\left(\frac{\Phi}{3}\right) - \frac{U}{3} \tag{27}$$

$$Z_2 = 2\Theta^{(1/3)}\cos\left(\frac{\Phi}{3} + \frac{2\pi}{3}\right) - \frac{U}{3} \tag{28}$$

$$Z_3 = 2\Theta^{(1/3)}\cos\left(\frac{\Phi}{3} + \frac{4\pi}{3}\right) - \frac{U}{3} \tag{29}$$

The largest and smallest are the vapour and liquid phases, respectively. The middle one has no physical interpretation.

Nomenclature

Latin symbols

$\mathcal{L}$	log-likelihood function
A	total cross section of the bed
A_f	cross section of the bed occupied by the fluid
c_f	concentration of solute in fluid phase
c_f^*	concentration of solute at the solid–fluid interface
c_p	concentration of solute in the core of a pore
c_s	concentration of solute in solid phase
c_s^*	concentration of solute at the solid–fluid interface
c_{f0}	inital concentration of solute in fluid phase
c_{pf}	concentration of solute in the pore opening
c_{s0}	inital concentration of solute in solid phase
D_e^M	axial diffusion coefficient
D_i	internal diffusion coefficient
D_i^R	reference value of internal diffusion coefficient
e	internal energy
F	mass flow rate
G	vector of discretized differential equations
k_m	mass partition coefficient
k_p	volumetric partition coefficient
L	length of fixed bed
l	characterisitic dimension of particles
P	pressure
p	probability distribution model
r	particle radius
R_e	Reynolds number
r_e	mass transfer kinetic term
T	temperature
t	time
T^{in}	inlet temperature
T^{out}	outlet temperature
t_0	inital extraction time
t_f	total extraction time
u	superfical velocity
v	linear velocity
x	state vector
Y	yield measurment
y	extraction yield
z	spatial direction

Greek symbols

ϵ	unobservable error
γ	decaying function
μ	sphericity coefficient
Φ	bed porosity
ρ_f	fluid density
ρ_s	bulk density of solid
σ	standard deviation
Θ	paramter space
θ	vector of unknown parameters
Υ	decay coefficient

Abberivations

BIC	broken-and-intact cell model
HBD	hot ball diffusion
MLE	maximum likelihood estimation
SC	shrinking core
SFE	supercritical fluid extraction